Soft Matter

PAPER

View Article Online
View Journal | View Issue

Cite this: *Soft Matter*, 2016, **12**, 1868

Filamentous supramolecular structures with polyelectrolyte and cadmium sulfide

J. Düring and F. Gröhn*

Received 19th November 2015,
Accepted 2nd December 2015

DOI: 10.1039/c5sm02840j

www.rsc.org/softmatter

In this study, a new type of filamentous structures consisting of a generation 9 poly(amido amine) dendrimer (G9) and CdS is reported. The linearity of the interconnected dendrimers is a result of the electrostatic repulsion between the multiply charged dendrimer macroions. Structures have been investigated by dynamic light scattering (DLS) and transmission electron microscopy (TEM). The internal structure of the CdS-fibers reveals information on the mechanism of the fiber formation. In contrast to previous systems with smaller generation poly(propylene imine)-dendrimers, Cd^{2+} is here found to be responsible for the interconnection of G9. Furthermore, more complex supramolecular structures were built by associating the CdS–dendrimer hybrid fibers with different ionic dyes, displaying the versatility of this system for future nanotechnology applications such as optoelectronics or energy conversion.

Introduction

In terms of miniaturizing devices modern technology makes more and more use of nanostructured systems and developing concepts for their creation, for example by self-assembly, becomes more and more important.[1] One dimensional (1D) nanostructures are of particular interest for electronic and optoelectronic applications, such as nanowire field-effect transistors[2] or multi-color nanophotonics with 1D silicon and 1D semiconducting nanocrystals.[3] Also spherical nanoparticles can form 1D structures *via* self-assembly and show promising properties for biomedical applications.[4] Fibroid structures can be applied to diverse purposes, for example water purification by nano-fibrous membranes made of polysaccharide.[5] Nevertheless, the production of 1D structures is rather challenging, as shape, size and monodispersity have to be controlled. Different strategies are possible to achieve anisotropic growth. Several nanolithographic techniques are accessible,[6,7] which are, however, rather cost intensive and difficult to scale up. Therefore, high potential lies in the development of wet chemical synthesis strategies to prepare the desired structures. Various template-directed syntheses,[8] including filamentous viruses,[9] have been reported, as well as kinetic control over the morphology *via* appropriate capping agents[10] and self-assembly of nanoparticles.[11] In terms of self-assembly, recently the possibility of dendrimeric macromolecules to assemble into fibrous structures under certain reaction conditions has been shown. The process of fiber-formation with poly(propylene imine) (PPI) dendrimer of the fourth generation (G4) and cadmium acetate was discussed by Fahmi *et al.* and Garzoni *et al.*[12,13] On the one hand, a mechanism was proposed which is based on the flexibility of the G4 dendrimer becoming interconnected by Cd^{2+}, yielding fibers that can subsequently be turned into chains of CdSe nanoparticles connected by dendrimer macromolecules.[12] On the other hand, Garzoni suggests that the reason for fiber formation lies in the hydrophobic effect of the acetate counterion, which induces anisotropy within the dendrimer.[13]

In the present study a system of a poly(amido amine) (PAMAM) dendrimer of the ninth generation (G9) in combination with cadmium nitrate and sodium sulfide was investigated, yielding fibrous structures. Subsequently, the fibers were further interconnected by ionic dye molecules leading to a novel type of ternary nanoparticle–dendrimer–dye supramolecular structure. It should be pointed out that in the system investigated herein the hydrophilic nitrate is used as the counterion in combination with a spherical G9 dendrimer not exhibiting the flexibility of a G4 dendrimer. Hence, due to component polarity and building block size and flexibility, a fundamentally different origin of the fiber formation than suggested previously must exist in the system investigated here.

Experimental

Materials

The poly(amido amine) dendrimer of generation 9 (G9) was supplied by Dendritech, Midland, MI and all other chemicals were purchased from Sigma-Aldrich. The azo dye Ar26 was purified prior to use *via* recrystallization (96%). To remove dust-particles for the light scattering measurements, the deionized water was filtered

Department of Chemistry and Pharmacy and Interdisciplinary Center for Molecular Materials (ICMM), Friedrich-Alexander-University Erlangen-Nürnberg, Egerlandstraße 3, 91058 Erlangen, Germany. E-mail: franziska.groehn@fau.de

with two cellulose acetate membranes in a row, which had a pore size of 0.22 μm.

Sample preparation

Aqueous stock solutions of all chemicals were prepared without further adjustment of the pH value. The Na_2S solution was always at maximum one day old and was stored at 4 °C. The CdS-fiber samples were prepared by first mixing aqueous solutions of G9 PAMAM dendrimer with $Cd(NO_3)_2$ at room temperature *via* stirring at 990 rpm. This solution had concentrations of $c(G9) = 2.3\times10^{-6}$ mol L^{-1} and $c(Cd(NO_3)_2) = 9.6 \times 10^{-4}$ mol L^{-1} and was stirred for 15 minutes before a freshly prepared aqueous solution of Na_2S was added to mineralize CdS nanoparticles, giving slightly yellow solutions with a final volume of 1–3 mL. The final sample had concentrations of $c(G9) = 1.7 \times 10^{-6}$ mol L^{-1}, $c(Cd(NO_3)_2) = 7.1 \times 10^{-4}$ mol L^{-1} and $c(Na_2S) = 1.1 \times 10^{-3}$ mol L^{-1}. The interconnection with dye was usually performed by diluting the fiber-sample and adding appropriate amounts of dye *via* stirring at 990 rpm, giving a final concentration of $c(G9) = 2.0 \times 10^{-7}$ mol L^{-1}.

Methods

Light scattering. The measurements were performed at an instrument which was equipped with a red HeNe laser (λ = 632.8 nm; 20 mW), an ALV 5000 correlator with 320 channels (ALV GmbH, Langen, Germany) and an ALV CGS 3 goniometer. The measurements covered an angular range of $30° \leq \theta \leq 150°$. The intensity autocorrelation function $g_2(\tau)$ was for each angle transferred into the electric field autocorrelation function $g_1(\tau)$ *via* the Siegert relation. The electric field autocorrelation function $g_1(\tau)$ was successively transformed into the distribution of relaxation times $A(\tau)$ by a regularized inverse Laplace transformation using the program CONTIN developed by S. Provencher.[14] From the distribution of relaxation times the apparent diffusion coefficient was calculated and *via* extrapolation to zero scattering vector square the diffusion coefficient was obtained, with which *via* Stokes–Einstein relation the hydrodynamic radius was calculated. To suppress the polyelectrolyte effect, the measurement of the pure G9 dendrimer and the G9 + $Cd(NO_3)_2$ sample (Fig. 2) were performed in a 0.14 mM NaCl solution.

UV-Vis spectroscopy. Absorption spectra were recorded on a SHIMADZU UV Spectrophotometer (UV-1800) with a slit width of 1.0 nm. For all measurements 10 mm quartz cuvettes were used. The size determination of CdS nanoparticles was performed *via* the Henglein equation[15–17] through the tangent at the onset of the absorption.

Fluorescence spectroscopy. Emission measurements were recorded using a FluoroMax-3 from Horiba Scientific (excitation wavelength λ = 350 nm).

TEM. The transmission electron microscopy (TEM) images were acquired with a Zeiss EM 900 microscope, operated at 80 kV at magnifications ranging from 20 000× to 250 000×. The specimens were prepared by depositing 5 μL of the diluted sample solution onto carbon-coated copper grids, 300 mesh, and air-dry the grids.

Results and discussion

The CdS-fibers are prepared by first mixing aqueous solutions of G9 PAMAM dendrimer with $Cd(NO_3)_2$ at room temperature. This solution is stirred for 15 minutes before a freshly prepared aqueous solution of Na_2S is added to mineralize CdS nanoparticles. After the addition of Na_2S the solution turns slightly yellow and the formation of CdS nanostructures can be confirmed with UV-Vis and fluorescence spectroscopy (Fig. 1a). The fibers are investigated with dynamic light scattering (DLS, Fig. 1b) and transmission electron microscopy (TEM, Fig. 1c and d). The DLS measurement results in two radii of 11 nm and 100 nm and the TEM measurement shows 2–10 nm thick fibers of several hundred nanometer to micrometer length.

Insight into the structure formation and the origin of the fibrous architecture can be gained by variation of the composition parameters and preparation route. It turns out that the final concentration of the G9 has to be at least 1.5×10^{-6} mol L^{-1}. Below that concentration, no fibers are formed, but solely single CdS particles result that are stabilized by the dendrimer. With higher concentrations of G9 (tested up to $c(G9) = 1.1 \times 10^{-5}$ mol L^{-1}) the concentration of the fibers increases,[19] but the structure of the fibers itself does not change. Thus, the structure is determined by the building blocks and not (entirely) kinetically. Interestingly, when Na_2S is added prior to Cd^{2+}, no fibers are formed. This shows the important role cadmium plays in the interconnection of the dendrimer. In addition, the ratio between the Cd salt and the dendrimer plays a decisive role. The coordination loading ratio of Cd^{2+} to G9 is herein defined as the ratio of four times the molar concentration of cadmium to the molar concentration of the primary amine groups of the dendrimer:

$$l_{\mathrm{coord}}(\mathrm{Cd/G9}) = \frac{4 \cdot c(\mathrm{Cd^{2+}})}{c(\mathrm{NH_2, dendrimer})}$$

This is due to the fact that four primary amine groups of the dendrimer coordinate to the Cd^{2+}.[20,21] The coordination loading ratio of the cadmium nitrate to the G9 dendrimer was changed from 0.6 to 1.4. At a loading ratio of $l_{coord}(Cd/G9) = 0.6$, again only single CdS particles are stabilized by the dendrimer. Starting with a loading ratio of $l_{coord}(Cd/G9) = 0.8$, filamentous structures can be seen in TEM measurements after the mineralization of CdS with Na_2S solution. With further increasing the loading ratio, larger structures can be found with light scattering measurements. The thickness of the fibers stays constant, only the length and with that, the overall size of the fiber bundles increases, as can be detected by TEM. At all investigated loading ratios there is free CdS-loaded dendrimer present in solution, which is visible in TEM. With higher loading ratio of cadmium nitrate to G9, this coexisting free dendrimer forms aggregates additionally to the fibers. This trend can also be observed with DLS (see Fig. 1b). The first distinct peak at small decay time is due to free dendrimer and aggregates out of these, whereas the second peak at larger decay times is caused by the fiber bundles. Both species increase in size with increasing loading ratio, the aggregates increase from 8.5 nm to 22 nm and the fiber bundles from 94 nm to 119 nm (not shown).

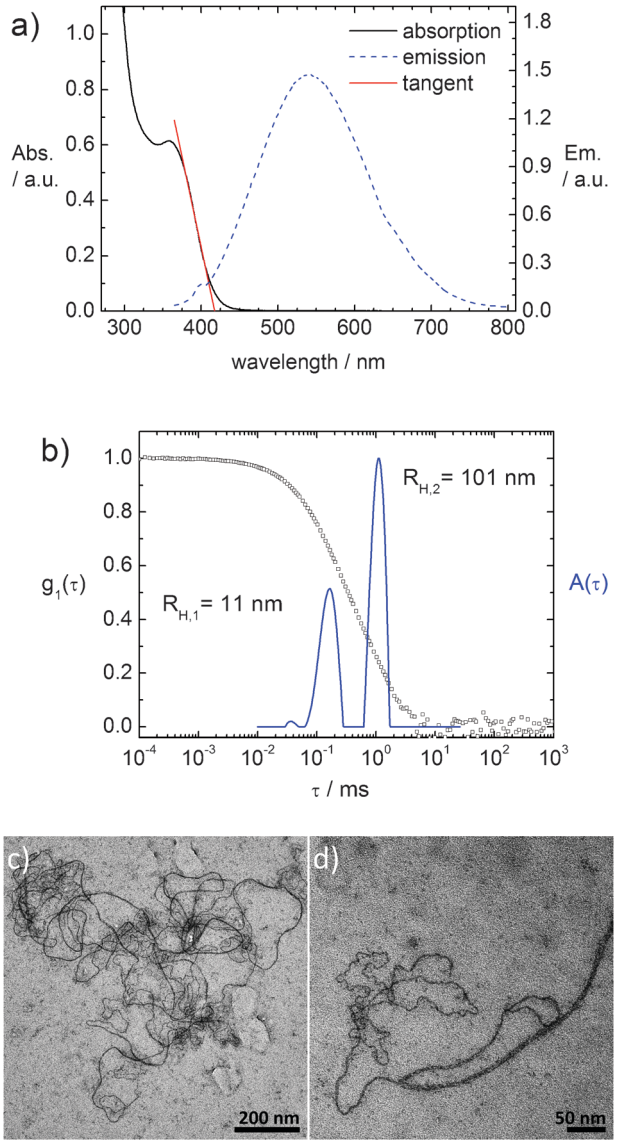

Fig. 1 Investigation of CdS-fiber samples: (a) absorption and emission spectrum of a CdS-fiber sample with l_{coord}(Cd/G9) = 0.9. The size of the CdS particles can be determined with the tangent at the onset of the absorption to d = 2.4 nm. The emission maximum is at λ_{em} = 540 nm (λ_{exc} = 350 nm).[18] (b) Dynamic light scattering: electric field autocorrelation function $g_1(\tau)$ with distribution of relaxation times $A(\tau)$ at a scattering angle of Θ = 90° for a sample with l_{coord}(Cd/G9) = 1.0. The smaller peak is due to free dendrimer and small aggregates, the larger peak is caused by fibers. (c and d): TEM pictures of two fiber samples (both l_{coord}(Cd/G9) = 0.8) at different magnifications. The filamentous CdS structures are clearly visible, whereas the dendrimer macroions are not visible.

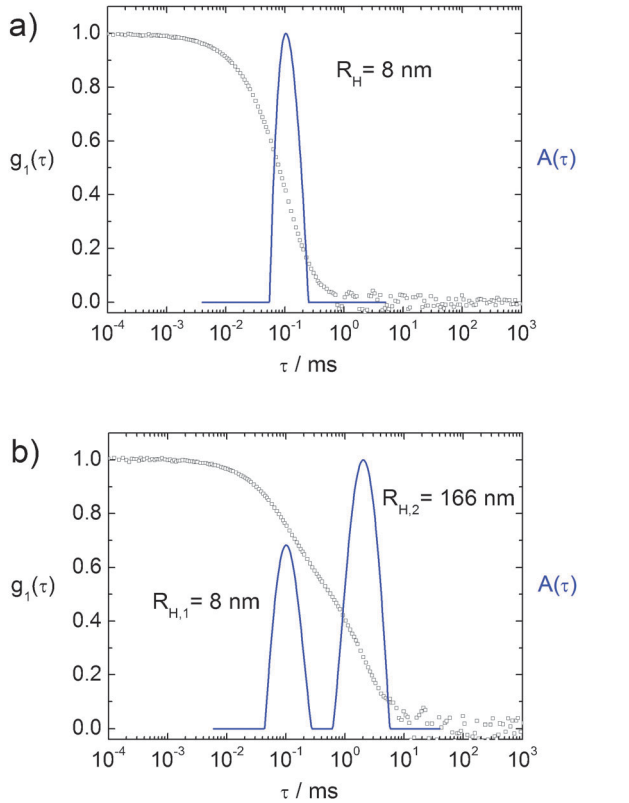

Fig. 2 Dynamic light scattering on (a) pure G9 dendrimer and (b) G9 + $Cd(NO_3)_2$ (l_{coord}(Cd/G9) = 1.0). Electric field autocorrelation function $g_1(\tau)$ with distribution of relaxation times $A(\tau)$ at a scattering angle of Θ = 90°. The concentration of G9 was in both times c(G9) = 4.3 × 10^{-6} mol L^{-1}.

To further elucidate the role of the Cd-ions, a combination of G9 dendrimer and the cadmium salt only in solution were investigated: in addition to individual dendrimers (8 nm), also larger structures form, as can be measured with DLS (Fig. 2a and b).

As the loading ratio of Cd to G9 has to be at least l_{coord}(Cd/G9) = 0.8, the primary amine outer "shell" of the dendrimer evidently has to be nearly fully coordinated with Cd^{2+} before fibers can form. Upon coordination the primary amine groups release their proton, as coordination is more favored than protonation. As a consequence, the nearly fully coordinated outer shell of the dendrimer carries only half the number of charges than without Cd^{2+}. (Four initially singly charged amine groups coordinate to one Cd^{2+}; *i.e.* four charges convert into two charges.) Additionally, the ionic strength increases upon addition of $Cd(NO_3)_2$. Therefore, the overall charge of the dendrimer is screened and the macroions approach each other much closer than before the addition of the cadmium salt. Thus, upon random collision, the Cd^{2+} can interconnect two dendrimers. When more dendrimers come into contact, interconnection proceeds. A linear chain forms, because all dendrimers are multiply charged and therefore repel each other. The largest distance between all interconnected dendrimer macroions can result from the formation of linear chains (Scheme 1).

To determine the role of the counterion, in a further experiment $CdCl_2$ was used as the Cd^{2+} source. Similar fiber structures were obtained with $CdCl_2$ after the addition of Na_2S, proving that not the kind of counterion but only the cadmium and the existence of any kind of screening counterion is important in this system. The influence of the ionic strength and thus screening of the dendrimer macroions can be elucidated by the addition of NaCl to a solution of G9 and $Cd(NO_3)_2$. The scattering intensity in light scattering experiments increases with increasing amount of added salt. This can be understood in the way that the G9 can come more easily into contact with each other

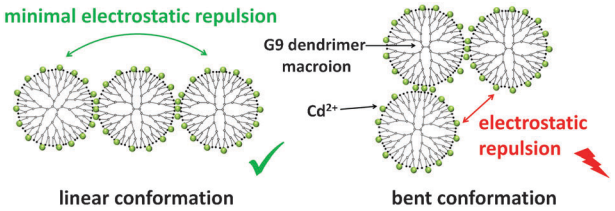

Scheme 1 Schematic representation for the preferred linear chain formation of G9 and Cd^{2+} due to electrostatic repulsion between the multiply charged G9 macroions.

and interconnects more, resulting in a higher scattering intensity. If no sulfide is added to a solution of G9 and Cd^{2+}, the interconnection of the dendrimers continues until, (within few days), the sample precipitates. Upon addition of Na_2S, CdS nanoparticles are formed and the Cd^{2+} is no longer able to interconnect the dendrimer any further. Thus the growth is stopped and the sample is stable in solution. At higher loading ratios of Cd to G9 more counterions are in solution, increasing the screening effect. Therefore not only are more and longer fibers formed, but also additional undirectional aggregation takes place, as can be seen in DLS and TEM measurements (not shown).

Discussion of the fiber structure

At all investigated loading ratios where fibers are formed, one can find two coexisting kinds of fibers. On the one hand there are thick and rather inflexible ''double-fibers'', which appear to consist out of two fibers lying in very close proximity next to each other (on the left side in Fig. 3) and on the other hand there are rather thin and quite flexible single-fibers (on the right side in Fig. 3). The visible thickness of these threads is about 2–3 nm, thus in the size range of single CdS nanoparticles (size determination *via* UV-Vis spectroscopy, see Fig. 1a).

Single-fibers. In some spots in the TEM picture of Fig. 3 a single-fiber appears to wrap around the G9 dendrimer, which has a size of 13 nm (red arrows). The CdS likely forms near the surface of the dendrimer, as Cd^{2+} mainly interacts with the primary amine groups.[22,23] As the G9 dendrimer with 13 nm is quite large compared to the visible CdS particles (2–3 nm), it is impossible, due to steric reasons, that only one CdS particle

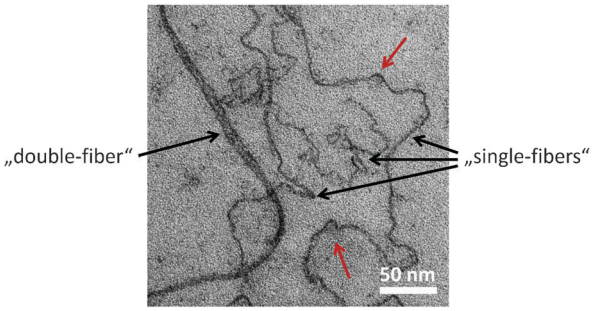

Fig. 3 TEM image of a sample with l_{coord}(Cd/G9) = 0.8, l(S/Cd) = 0.5 with single fibers (right side) and a double fiber (left side) depicted. The red arrows mark spots, where gray circles might represent G9 macromolecules with a CdS single-fiber wrapping around the surface.

is attached to one dendrimer in the chain. Fahmi *et al.*[12] gave an interpretation of a conformational change towards a more anisotropic dendrimer structure in a system with generation 4 PPI dendrimer. This, however, is not possible in the system investigated herein: due to the size and the strong branching of a ninth generation dendrimer, the G9 is not as flexible and therefore, unlike smaller generation dendrimers, retains its spherical shape[24,25] where it is impossible to locate all primary amino groups on the poles of the dendrimer. An interpretation given by Garzoni *et al.*[13] is based on the counterion acetate from $Cd(CH_3COO)_2$, introducing anisotropy to the generation 4 PPI dendrimer due to hydrophobicity and thus causing fiber formation. As in the present study nitrate was used as counterion, having no hydrophobic properties, this cannot be the case here either. Most importantly, the structure of the CdS fibers found here rules out the previously suggested explanations. The width of the threads is much smaller than the G9 dendrimer and the distance between the single CdS particles is also smaller than the diameter of G9 (from continuous fiber to max. 7 nm, diameter of G9 = 13 nm). The only plausible explanation for the fiber structure found herein is that the fiber growth proceeds along the surface of one G9 molecule to the next one, forming a kind of CdS ''backbone'', consisting of CdS nanoparticles. The conformational change of the G9 dendrimer is small but sufficiently high, so that a straight fiber of CdS particles can form without the curvature of G9 being visible everywhere. This is confirmed by TEM pictures of a stained sample (Fig. 4a and b), TEM pictures of higher magnification (Fig. 4c and 5c) and illustrated in the following scheme (Fig. 4d). In Fig. 4a the TEM picture of a fiber sample is shown, which was stained with phosphotungstate $Na_3PW_{12}O_{40}$. Fig. 4b shows the proposed positions of the G9 macromolecules in relation to the CdS fiber.

Double-fibers. The second kind of fiber, coexisting with the thin flexible ones are thicker and rather inflexible double-fibers, which appear to consist out of two fibers lying in very close proximity next to each other. The visible thickness of the double-fibers ranges from 4 nm to about 10 nm. The majority lies in the range of 7 nm. The gap between the two fibers amounts from a maximum of 4 nm to zero where the two fibers fuse into one. The diameter of one G9 molecule in solution is about 13 nm. This could mean that both threads in the double fibers run along the same G9 molecules, aligned as a chain of beads. So theoretically, the maximal gap between the two fibers could be 7 nm (assuming 3 nm large CdS particles, embedded oppositely in the surface of 13 nm large G9). The observed smaller gap of 4 nm and the smaller total thickness of 10 nm instead of 13 nm might be understood by the shrinkage of the G9 upon drying on the TEM-grid surface. The merge of the two fibers, which is observed quite often (see also Fig. 3), can be understood by a twist of the fiber chains as illustrated in Fig. 5d. Thus the two CdS fibers lie on top of each other and are visible as only ''one fiber'' with slightly higher contrast.

To understand why the CdS particles are not randomly distributed over the G9 surface, but lie in a line one has to consider different effects. At first Hamaker interaction (the van der Waals interaction in colloidal systems) leads to attraction of

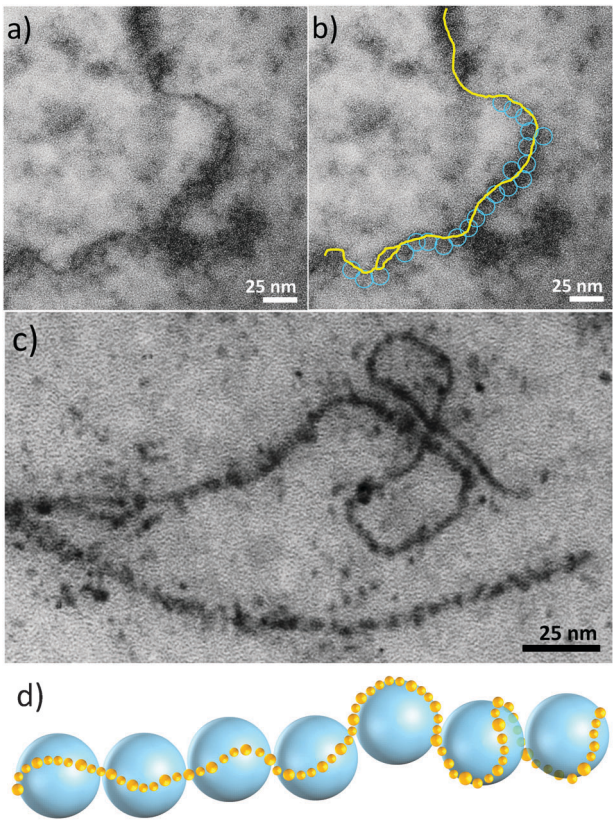

Fig. 4 (a) TEM picture of a CdS-fiber sample and (b) the same picture with the proposed orientation of CdS and G9 dendrimer. The yellow line symbolizes the CdS thread and the blue circles represent the G9 macromolecules. The sample was stained with $Na_3PW_{12}O_{40}$. (c) TEM picture of a CdS-fiber sample with higher magnification, where single CdS nanoparticles are visible along the fiber. (d) Scheme of the proposed structure of a thin CdS fiber (yellow, 2–3 nm) proceeding along G9 surfaces (large blue spheres, 13 nm).

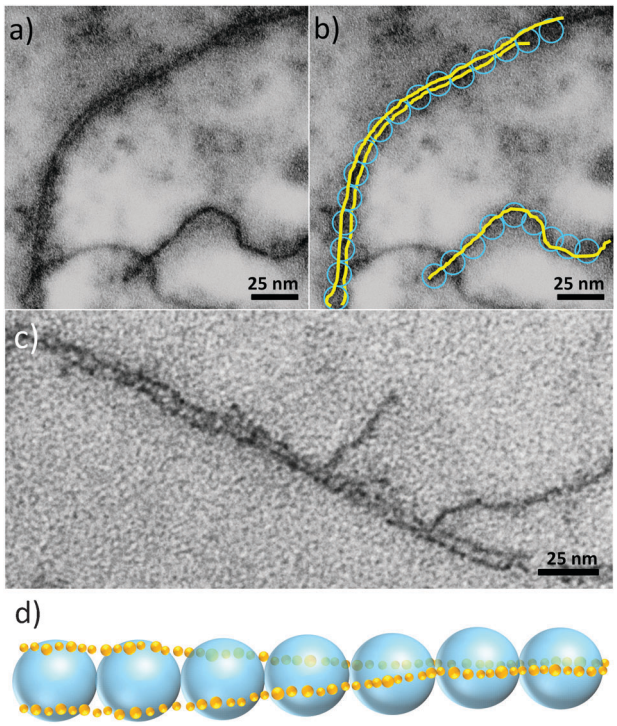

Fig. 5 (a) TEM picture of a CdS-fiber sample and (b) the same picture with the proposed orientation of CdS (yellow) and the G9 dendrimer (blue circles). The sample was stained with $Na_3PW_{12}O_{40}$. (c) TEM picture of a CdS-fiber sample with higher magnification, where single CdS nanoparticles are visible along the double-fiber. (d) Scheme of a CdS double fiber, formed by a single G9 bead chain with twist. Large blue spheres symbolize 13 nm G9, small yellow spheres symbolize 2–3 nm CdS.

the CdS nanoparticles.[26] Next, the stabilization of the CdS surface with primary amine groups has to be considered as this is presumably the reason for the small size (2–3 nm) of the single CdS particles. The primary amine groups in the vicinity of a CdS particle are bound to its surface. The next CdS particle tends to be close to the first one (due to Hamaker interaction) which leads to a decrease in the amount of primary amine groups in between these two particles. Therefore a third and fourth particle can be better stabilized by amine groups at the longitudinal ends and not in the region where the first two particles are close. This results in the CdS particles arranging in line. A further effect that might play a role could be the counterion distribution around the dendrimer.[27] Once the first particle has formed, the Cd^{2+} charges are neutralized in this area. Therefore the ionic strength in vicinity of the CdS is weaker than at the rest of the macromolecule. This facilitates the S^{2-} ions to come into contact with further Cd^{2+} ions to form the next CdS particle. The formation of the first CdS particle of each G9 dendrimer most likely takes place somewhere at the equator of the G9. At the poles, where the G9 is interconnected to the next G9 macromolecule, the Cd^{2+} has a chance to be higher coordinated and is thus more strongly bound. Also due to steric effects it is unlikely that CdS crystallizes there first. Thus, the CdS chain starts at every G9 dendrimer near the equator and proceeds towards the poles. Due to the spherical shape of the dendrimer, the CdS chain segments can meet at the poles and form a continuous CdS-particle-fiber.

Thus, the mechanism of the CdS fiber formation can be understood by the following steps: first the interconnection of single G9 by Cd^{2+} takes place. The electrostatic repulsion between the single G9 polyelectrolytes causes the linearity of the assemblies. After addition of S^{2-}, CdS nanoparticles form along the preformed linear structure proceeding along the surface of the dendrimer due to Hamaker interaction and possibly primary amine group a decrease in the amount, counterion interaction and geometric effects. Where the concentration of Cd^{2+} is higher due to slight inhomogeneity the CdS nanoparticles form on opposing sides of the G9 resulting in stiffer double-fibers.

It cannot be fully excluded that the CdS nanoparticles are in some places grown together within the fiber structure. From TEM images with high magnification, intermissions and single particles are visible in many places along the fibers, as can be seen in Fig. 4c and 5c, confirming the fiber formation as described above.

Interconnection of fibers with an ionic dye

For functional applications for example in catalysis or solar cells it is often desirable to combine more than two components in a composite nanostructure, preferably through the facile and

versatile route of self-assembly. As we have reported previously, it is possible to form binary supramolecular structures from polyelectrolytes and multivalent oppositely charged dye molecules.[28] Currently we could show that the principle can be extended to dendrimers containing an inorganic nanoparticle.[29] It is now of high interest whether the approach of ionic-dye-interconnection can be transferred to the much larger and already more complex CdS–dendrimer hybrid fibers. On that account the fibers were combined with the divalent anionic dye Acid Red 26 (Ar26) and the resulting supramolecular structures were investigated.

The loading ratio between a charged dye and the dendrimer is defined as the molar concentration of charges of the dye to the molar concentration of charges of the dendrimer:

$$l(\text{dye/G9}) = \frac{c(\text{dye}) \cdot \text{charge dye}}{c(\text{G9}) \cdot \text{primary amine groups}} = \frac{c(\text{dye}) \cdot 2}{c(\text{G9}) \cdot 2048}$$

At rather low ratios between Ar26 and G9 (l(Ar26/G9) = 0.5) the radius of the structures decreases in comparison to the pure fibers from R_h = 151 nm to R_h = 73 nm. This is rather unexpected, as an interconnection of the fiber structures should lead to larger supramolecular assemblies. But in TEM it becomes evident that the dye causes the fibers to conglobate and that the free dendrimer, which coexists with the fibers, is also interconnected to rather spherical assemblies as can be seen in Fig. 7a. The width of distribution becomes smaller for the interconnected fiber sample, which can be understood by the coagulation of the fibers resulting in denser and more defined super-structures. Additionally the assemblies of the free dendrimer, which are in the same size range as the conglobate fibers, now also contribute to the scattering intensity, with that narrowing down the width of distribution from σ = 0.23 for the pure fiber sample to σ = 0.17 for the interconnected sample (Fig. 6).

One can also observe that the thin fiber parts are more agglomerated than the thick double fibers. This is reasonable, as the thin fibers are flexible enough to globe, but the double fibers are rather stiff and cannot bend in such a way and then be hold in this position by the Ar26.

For higher loading ratios of Ar26 to G9 (l(Ar26/G9) > 0.71) the fibers are connected with each other and form large structures. With DLS large aggregates of R_h = 613 nm and a width of distribution of σ = 0.3 can be found for l(Ar26/G9) = 0.75. With TEM it becomes evident that the aggregates do not only consist of fibers, but again the free dendrimer constitutes a large part of these assemblies (Fig. 7d). Even larger assemblies of several micrometers are found in this measurement (Fig. 7c), as the TEM grid was prepared after the light scattering measurement. It is difficult to obtain stable aggregates consisting out of interconnected fibers, as these structures usually grow with time and start to precipitate after a while. Nevertheless, it is possible to investigate those samples, before they precipitate.

This interconnection behavior is not limited to Ar26, but can also be found for the dye Acid Red 94 (Ar94, also known as Rose Bengal) (see Scheme 2). The dependence of the hydrodynamic radius of the assemblies on the loading ratio of Ar94/G9 is depicted in Fig. 8. At loading ratios of 0.2 and 0.35 the sizes of the resulting structures are smaller than the pure fibers. This

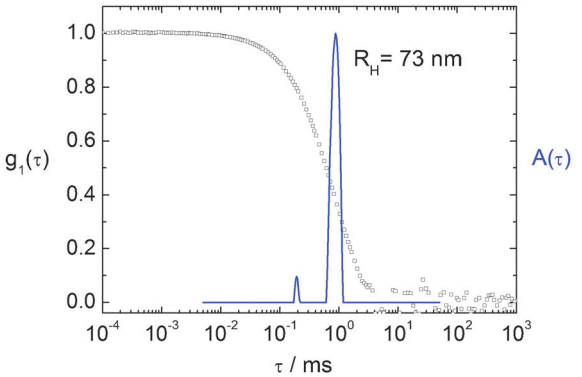

Fig. 6 Dynamic light scattering on a CdS-fiber sample with Ar26: electric field autocorrelation function $g_1(\tau)$ with distribution of relaxation times $A(\tau)$ at a scattering angle of Θ = 90°. Width of distribution σ = 0.17, R_h = 73 nm. Sample specifications: l(Ar26/G9) = 0.5; l_{coord}(Cd/G9) = 0.8.

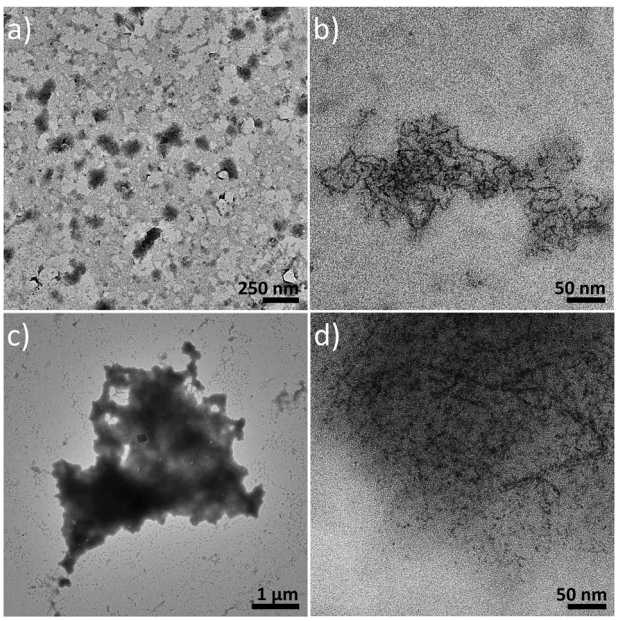

Fig. 7 TEM pictures of a CdS-fiber samples with Ar26. (a and b) Lower loading ratio of l(Ar26/G9) = 0.5; (c and d) higher loading ratio of l(Ar26/Cd) = 0.75, all l_{coord}(Cd/G9) = 0.8. (a) Several assemblies of previously free dendrimer with sizes of about 150 nm; (b) conglobated fiber. (c) Ar26-fiber aggregate; (d) larger magnification with filamentous structure being visible alongside free dendrimer.

result is in analogy to the before mentioned Ar26 system, and can be explained with the conglobation of the single fibers. Starting from l(Ar94/G9) = 0.4 the size increases with increasing loading ratio and for l(Ar94/G9) > 0.6 the sample precipitates after short time. Around l(Ar94/G9) = 0.5 stable aggregates form. Thus, versatile structures are accessible with CdS-fibers and different dyes. The behavior of the system is understood and therefore predictable also for new dyes, expanding the range of possible future applications.

Further, it was tested whether these CdS-fibers can also build the basis of a light responsive system. The dye Acid Yellow 38 (Ay38) is light switchable and upon irradiation transforms from the *trans*- to the *cis*-isomer (see Scheme 2). This property can be

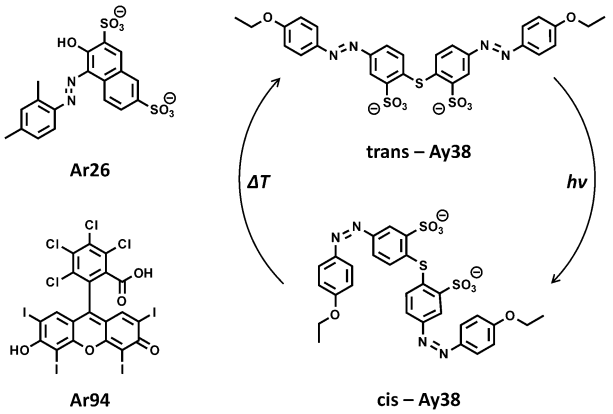

Scheme 2 Dye molecules used to interconnect CdS–dendrimer fibers to supramolecular assemblies.

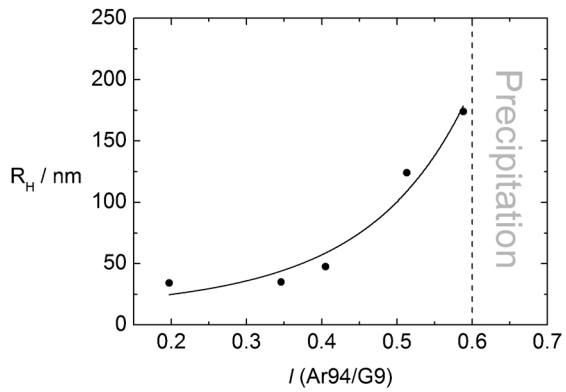

Fig. 8 Dependence of the hydrodynamic radius of the fiber–dye aggregates on the loading ratio *l*(Ar94/G9).

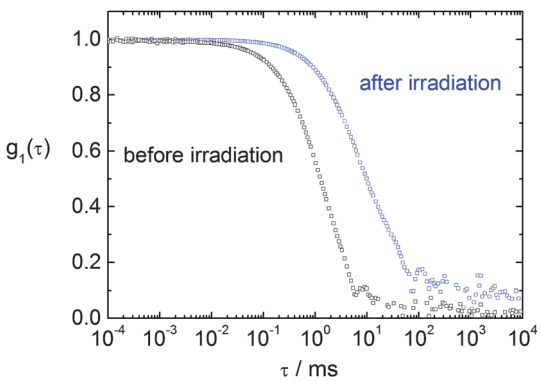

Fig. 9 Dynamic light scattering on a CdS-fiber sample with Ay38: electric field autocorrelation functions $g_1(\tau)$ at scattering angles of $\Theta = 60°$. Black curve: non-irradiated sample, blue curve: same sample after 20 min irradiation at λ = 380 nm. Sample specifications: *l*(Ay38/G9) = 2.5; l_{coord}(Cd/G9) = 0.9.

used to build supramolecular assemblies that respond to irradiation with a change in size as shown previously.[30] In the case of understoichiometric loading ratio no size change of the supramolecular assemblies can be observed upon irradiation, whereas for overstoichiometric loaded samples a strong increase in assembly size is observed, as can be seen in Fig. 9.

It turned out that the CdS–dendrimer hybrid fibers show a behavior corresponding to the purely organic dendrimer–dye structures. Thus it can be concluded that for electrostatic self-assembly of the CdS–dendrimer fiber system similar possibilities are accessible as for the pure dendrimer, giving rise to various new size tunable multicomponent organic–inorganic supramolecular structures and switchable systems.

Conclusions

In summary, filamentous organic–inorganic hybrid structures can be formed with generation 9 PAMAM dendrimer, cadmium nitrate and sodium sulfide. The cadmium ion is responsible for the interconnection of the polyelectrolytes and the electrostatic repulsion between the dendrimers causes linear structures. With the addition of sodium sulfide, CdS mineralizes along the preformed fiber, resulting in filamentous organic–inorganic hybrid structures. It was exemplarily demonstrated that the remarkable properties of the dendrimer are still accessible, such as the ability to interconnect with various ionic dyes to size tunable assemblies or the interaction with a light responsive dye giving light switchable nanosystems. Thus, various supramolecular systems can be created based on the CdS–dendrimer fibers as a building block. The simplicity and versatility of the preparation of this system offer powerful tools for potential future applications for example in the fields of optoelectronics or solar energy conversion.

Acknowledgements

Financial support of Deutsche Forschungsgemeinschaft (DFG), the Interdisciplinary Center for Molecular Materials (ICMM, University Erlangen-Nürnberg) and Solar Technologies go Hybrid (SolTech) is gratefully acknowledged.

Notes and references

1 (*a*) D. J. Pochan, Z. Y. Chen, H. G. Cui, K. Hales, K. Qi and K. L. Wooley, *Science*, 2004, **306**, 94; (*b*) D. Hinderberger, O. Schmelz and M. Rehahn, *Angew. Chem., Int. Ed.*, 2004, **43**, 4616; (*c*) M. M. J. Smulders, A. P. H. J. Schenning and E. W. Meijer, *J. Am. Chem. Soc.*, 2008, **130**, 606; (*d*) S. Duschner, D. Störkle, M. Schmidt and M. Maskos, *Macromolecules*, 2008, **41**, 9067; (*e*) I. K. Voets, R. Fokkink, T. Hellweg, S. M. King, P. de Waard, A. de Keizera and M. A. Cohen Stuart, *Soft Matter*, 2009, **5**, 999; (*f*) Y. Xu, S. Bolisetty, M. Ballauff and A. H. E. Müller, *J. Am. Chem. Soc.*, 2009, **131**, 1640; (*g*) P. C. DeMuth, X. Su, R. E. Samuel, P. T. Hammond and D. Irvine, *Adv. Mater.*, 2010, **22**, 4851; (*h*) M. Yan, J. Fresnais and J.-F. Berret, *Soft Matter*, 2010, **6**, 1997; (*i*) F. Gröhn, *Soft Matter*, 2010, **6**, 4296; (*j*) G. Gröger, W. Meyer-Zaika, C. Böttcher, F. Gröhn, C. Ruthard and C. Schmuck, *J. Am. Chem. Soc.*, 2011, **133**, 8961; (*k*) E. Kizilay, A. D. Dinsmore, D. A. Hoagland, L. Sun and P. L. Dubin, *Soft Matter*, 2013, **9**, 7320.

2 Y. Li, F. Qian, J. Xiang and C. M. Lieber, *Mater. Today*, 2006, **9**, 18.
3 Y. Huang, X. Duan and C. M. Lieber, *Small*, 2005, **1**, 142.
4 A. Fahmi, T. Pietsch, M. Bryszewska, J. C. Rodríguez-Cabello, A. Koceva-Chyla, F. J. Arias, M. A. Rodrigo and N. Gindy, *Adv. Funct. Mater.*, 2010, **20**, 1011.
5 H. Ma, C. Burger, B. S. Hsiao and B. Chu, *Biomacromolecules*, 2011, **12**, 970.
6 D. Wouters and U. Schubert, *Angew. Chem., Int. Ed.*, 2004, **43**, 2480.
7 S. Matsui and Y. Ochiai, *Nanotechnology*, 1996, **7**, 247.
8 (*a*) L. Dong, T. Hollis, B. A. Connolly, N. G. Wright, B. R. Horrocks and A. Houlton, *Adv. Mater.*, 2007, **19**, 1748; (*b*) M. Zhang, M. Drechsler and A. H. E. Müller, *Chem. Mater.*, 2004, **16**, 537; (*c*) N. Ostrov, G. Fichman, L. Adler-Abramovich and E. Gazit, *J. Nanosci. Nanotechnol.*, 2015, **15**, 556; (*d*) P. Atanasova, N. Stitz, S. Sanctis, J. H. M. Maurer, R. C. Hoffmann, S. Eiben, H. Jeske, J. J. Schneider and J. Bill, *Langmuir*, 2015, **31**, 3897.
9 (*a*) T. Sawada, S. Kang, J. Watanabe, H. Mihara and T. Serizawa, *ACS Macro Lett.*, 2014, **3**, 341; (*b*) E. Grelet, A. Moreno and R. Backov, *Langmuir*, 2011, **27**, 4334.
10 Y. Xia, P. Yang, Y. Sun, Y. Wu, B. Mayers, B. Gates, Y. Yin, F. Kim and H. Yan, *Adv. Mater.*, 2003, **15**, 353.
11 (*a*) M. Llusar and C. Sanchez, *Chem. Mater.*, 2008, **20**, 782; (*b*) R. R. Unwin, R. A. Cabanas, T. Yanagishima, T. R. Blower, H. Takahashi, G. P. C. Salmond, J. M. Edwardson, S. Fraden and E. Eiser, *Phys. Chem. Chem. Phys.*, 2015, **17**, 8194; (*c*) T. He, G. Abbineni, B. Cao and C. Mao, *Small*, 2010, **6**, 2230.
12 A. Fahmi, D. Appelhans, N. Cheval, T. Pietsch, C. Bellmann, N. Gindy and B. Voit, *Adv. Mater.*, 2011, **23**, 3289.
13 M. Garzoni, N. Cheval, A. Fahmi, A. Danani and G. M. Pavan, *J. Am. Chem. Soc.*, 2012, **134**, 3349.
14 S. W. Provencher, *Comput. Phys. Commun.*, 1982, **27**, 229.
15 L. Spanhel, M. Haase, H. Weller and A. Henglein, *J. Am. Chem. Soc.*, 1987, **109**, 5649.
16 M. Moffitt and A. Eisenberg, *Chem. Mater.*, 1995, **7**, 1178.
17 R. He, X. Qian, J. Yin, H. Xi, L. Bian and Z. Zhu, *Colloids Surf., A*, 2003, **220**, 151.
18 The peak at 700 nm, which is the second order Rayleigh scattering of water from using a diffraction grading as dispersive element in the monochromator, was removed.
19 Scattering intensity is higher for higher concentrations ($\ln I$(higher) = −4.62, $\ln I$(lower) = −6.34). In TEM, at the same dilution, more fiber-bundles are visible for the high concentration than for the lower concentration, indicating that more fibers are formed at higher concentrations.
20 Cd^{2+} coordinates 6-fold octahedral or 4-fold tetrahedral for large ligands.[21].
21 A. F. Holleman and N. Wiberg, *Lehrbuch der Anorganischen Chemie*, Walter de Gruyter, Berlin, 102nd edn, 2007, p. 1489.
22 X. C. Wu, A. M. Bittner and K. Kern, *J. Phys. Chem. B*, 2005, **109**, 230.
23 G. G. Guilbault and S. M. Billedeau, *J. Inorg. Nucl. Chem.*, 1972, **34**, 1167–1171.
24 T. J. Prosa, B. J. Bauer and E. J. Amis, *Macromolecules*, 2001, **34**, 4897.
25 P. K. Maiti, T. Cagın, G. Wang and W. A. Goddard, *Marcomolecules*, 2004, **37**, 6236.
26 Y. Min, M. Akbulut, K. Kristiansen, Y. Golan and J. Israelachvili, *Nat. Mater.*, 2008, **7**, 527.
27 E. Seyrek, P. L. Dubin, C. Tribet and E. A. Gamble, *Biomacromolecules*, 2003, **4**, 273.
28 (*a*) F. Gröhn, K. Klein and S. Brand, *Chem. – Eur. J.*, 2008, **14**, 6866; (*b*) I. Willerich and F. Gröhn, *Chem. – Eur. J.*, 2008, **14**, 9112; (*c*) F. Gröhn, *Macromol. Chem. Phys.*, 2008, **209**, 2295; (*d*) I. Willerich, H. Ritter and F. Gröhn, *J. Phys. Chem. B*, 2009, **113**, 3339; (*e*) Y. Li, U. H. Yildiz, K. Müllen and F. Gröhn, *Biomacromolecules*, 2009, **10**, 530; (*f*) C. Ruthard, M. Maskos, U. Kolb and F. Gröhn, *Macromolecules*, 2009, **42**, 830; (*g*) I. Willerich, Y. Li and F. Gröhn, *J. Phys. Chem. B*, 2010, **114**, 15466; (*h*) F. Gröhn, K. Klein and K. Koynov, *Macromol. Rapid Commun.*, 2010, **31**, 75; (*i*) I. Willerich and F. Gröhn, *J. Am. Chem. Soc.*, 2011, **133**, 20341; (*j*) I. Willerich, T. Schindler, H. Ritter and F. Gröhn, *Soft Matter*, 2011, **7**, 5444; (*k*) C. Ruthard, M. Schmidt and F. Gröhn, *Macromol. Rapid Commun.*, 2011, **32**, 706.
29 J. Düring, A. Hölzer, U. Kolb, R. Branscheid and F. Gröhn, *Angew. Chem., Int. Ed.*, 2013, **52**, 8742.
30 (*a*) I. Willerich and F. Gröhn, *Angew. Chem., Int. Ed.*, 2010, **49**, 8104; (*b*) I. Willerich and F. Gröhn, *Macromolecules*, 2011, **44**, 4452; (*c*) D. Moldenhauer and F. Gröhn, *J. Polym. Sci., Part B: Polym. Phys.*, 2013, **51**, 802.